

# A Surface and Appearance-based Next Best View System for Active Object Recognition

Pourya Hoseini<sup>a</sup>, Shuvo Kumar Paul<sup>b</sup>, Mircea Nicolescu and Monica Nicolescu

*Department of Computer Science and Engineering, University of Nevada, Reno, U.S.A.*

**Keywords:** Object Recognition, Active Vision, Next Best View, View Planning, Foreshortening, Classification Dissimilarity, Robotics.

**Abstract:** Active vision represents a set of techniques that attempt to incorporate new visual data by employing camera motion. Object recognition is one of the main areas where active vision can be particularly beneficial. In cases where recognition is uncertain, new perspectives of an object can help in improving the quality of observation and potentially the recognition. A key question, however, is from where to look at the object. Current approaches mostly consider creating an occupancy grid of known object voxels or imagining the entire object shape and appearance to determine the next camera pose. Another current trend is to show every possible object view to the vision system during the training time. These methods typically require multiple observations or considerable training data and time to effectively function. In this paper, a next best view system is proposed that takes into account only the initial surface shape and appearance of the object, and subsequently determines the next camera pose. Therefore, it is a single-shot method without the need to have any specifically made dataset for the training. Experimental validations prove the feasibility of the proposed method in finding good viewpoints while showing significant improvements in recognition performance.

## 1 INTRODUCTION

It is a necessity for an intelligent entity to sense its environment to act informed. One of the main perception mediums is vision. Despite being a heavily used sensing modality, a vision mechanism may face difficulties in capturing the most useful views for the specific task at hand. There can be many reasons for such issues, including occlusion, lack of discriminative features due to bad lighting or unfavorable viewpoints of the object, or insufficient image resolution. Active vision is an answer to those situations that tries to enhance the performance of the vision system by dynamically incorporating new visual sensory sources. Some application domains of active vision are three-dimensional (3D) object reconstruction and object recognition, the latter being the focus of our work. Active Object Recognition (AOR) has many uses in robotics (Paul et al., 2020), vision-based surveillance, etc. AOR procedures normally involve uncertainty evaluation, camera movement, matching, and information fusion (Hoseini et al., 2019a) and (Hoseini et al., 2019b). If the current recognition is

not certain enough, a camera is moved to observe the object from another viewpoint and to fuse the current and new information, usually classification decisions, from the matched objects in the views, in order to obtain improved results.

Regarding the camera movement, a primary question to answer is where and in what orientation a camera should be placed to fetch the next best view (NBV) of the object. Finding next best view is an ill-posed task, because the current viewpoint of the object is usually not sufficient to deterministically deduce the object shape and appearance from its other facets. Approaches to NBV are generally impacted by the specific application they are being employed for. In 3D reconstruction applications, a NBV that plans to acquire a chain of views that are aimed to explore unobserved voxels of objects might be an ideal option. In contrast, the next views in an object recognition application are desired to present new discriminative features, by which the object recognition performance can be enhanced. The number of planned views for object recognition is also intended to be as low as possible to reduce energy and time spent moving the cameras physically.

A deep belief network is presented in (Wu et al.,

<sup>a</sup>  <https://orcid.org/0000-0003-3473-9906>

<sup>b</sup>  <https://orcid.org/0000-0003-1791-3925>

2015) to “hallucinate” the whole object shape and appearance in the presence of occlusion to compute the recognition uncertainty in several predefined camera poses. The viewpoint with the least uncertainty is then selected. Although interesting, this idea has a major flaw in depending heavily on the estimation of the object shape and appearance, which can be a large source of errors. In contrary to (Wu et al., 2015), the work in (Doumanoglou et al., 2016) directly estimates the classification probabilities of different views instead of rendering their hypothetical object appearances to compute the information gain in each view. Despite overcoming the problem of computationally expensive renderings of hypothetical 3D objects, this approach requires 3D training data for every test object and performing classification and confidence estimation for every viewpoint of the 3D objects in the training. This prerequisite significantly affects the functionality of the technique due to the scarcity of such training data for many real-world objects.

A boosting technique is proposed in (Jia et al., 2010) to combine three criteria for determining the NBV around objects. The first criterion compares the similarity of the current object with prerecorded object appearances in different views and selects the one with the least similarity. The other two criteria for choosing NBV are the prior probability of a viewpoint in successfully determining the object class given either a currently detected object pose or a currently detected object category. Aside from the priors, which are application data specific, using a similarity measure between the current viewpoint of an object and its other viewpoints requires a dataset made of images around the training objects with their known pose. This can be practically burdensome as there is a need to capture poses and appearances all around the objects that are to be detected at test time.

Rearranging depth camera positions based on imitating barn owls’ head motions is examined in (Barzilay et al., 2017) for 3D reconstruction of objects. The method in (Barzilay et al., 2017) mimics motions regardless of the object shape and appearance, which can cause missing some important clues in determining the next best view. In (Atanasov et al., 2014), an active pose estimation and object detection framework is described to balance the odds of object detection enhancement and the energy needed to move the camera. A multitude of captures are planned along the fastest way the camera is moved toward the object. Since the active vision system of (Atanasov et al., 2014) does not consider the object shape and appearance and merely moves the camera towards an object, it cannot be deemed as an intelligent viewpoint selection method.

A trajectory planning technique for an eye-in-hand vision system on a PR2 robot is presented in (Potthast and Sukhatme, 2011) to boost the expected number of voxel observation by searching for maximum local information gain. In continuation to the work of (Potthast and Sukhatme, 2011), a next best view method for 3D reconstruction applications on the basis of predicting information gain from prospective viewpoints is proposed in (Potthast and Sukhatme, 2014). To predict the information gain in unobserved areas, an occupancy grid is formed out of all the observations so far, and a Hidden Markov Model (HMM) is used to estimate the observation probability of unobserved cells in the grid.

By reviewing the literature, we see that the earlier work in determining the next best view is clustered in two groups: space occupancy-based and object estimation-based techniques. Assessing occupancy of 3D space via ray tracing and computation of information gain is intrinsically beneficial for 3D reconstruction purposes, because it attempts to discover more surface voxels than discriminative features for classification. That is why it has been preferred regularly in previous work for 3D reconstruction. In contrast, object estimation techniques depend on either “hallucinating” the 3D shape of the current object or comparing the current object shape and/or appearance to the ones acquired during training to infer the best camera pose by comparing different viewpoints. Their problem is, however, the reliance on large datasets of object images taken from predefined points of view as well as in the inaccuracies stemming from hypothetical object shapes/appearances.

In this paper, a single-shot next best view method for object recognition tasks is presented, which plans for one new viewpoint based on cues from the currently visible object shape and appearance to improve the object recognition performance when necessary. The proposed NBV method is neither reliant on a prior dataset of specifically designated images from around the object, nor on 3D object volumes for training. It uses conventional datasets, a collection of random images of objects, merely for the training of the classifiers. It also does not involve a chain of camera motions toward or around the object to save time and energy for camera motion. To achieve these characteristics, an ensemble of criteria is used to analyze different areas of the current view for appearance and shape cues to suggest a new camera pose. Examples of such criteria are classification dissimilarity between a region of the object image and the whole image, foreshortening, and various statistical texture metrics. A test dataset was also created to evaluate the proposed method in a systematic way. In the tests,

the proposed NBV system confirms its efficacy in predicting the next best camera view among a set of pre-selected test-time poses around the object. The main contributions of the proposed work are:

1. A novel next best system is proposed exclusively for the task of object recognition.
2. The current object shape and appearance are only used in the proposed NBV; hence no prior knowledge of objects is needed.
3. There is no need to create specially designed datasets for the next best view determination. The only training employed is for the object classifiers.
4. A small test dataset, comprised of the images captured around various objects, has been gathered to efficiently test the proposed NBV system. It can be used by other researchers as a benchmark.
5. Experimental validation shows good results in terms of the performance improvement after fusion of views among a pre-defined set of possible camera poses.

The remainder of the paper is organized as follows. The proposed next best view system is presented in section 2. Section 3 shows the results obtained in the benchmarks. Lastly, concluding remarks are discussed in section 4.

## 2 THE PROPOSED SINGLE-SHOT NEXT BEST VIEW METHOD

In order to find a candidate viewpoint in a single try after the initial capture, only the color and depth information of the initial camera view are assumed to be available. For rigorous testing purposes, the NBV poses are restricted to a number of pre-specified poses that are typically reachable for eye-in-hand or UAV platforms. The poses around any object are clustered into eight groups in the current implementation, all of them on the plane that passes through the object and is parallel to the image plane of the camera at the initial viewpoint. Each group is the set of poses that are generally viewing the same part of the object.

The viewpoints are selected to be at the same depth as the object in the camera coordinate of the initial view, because they can provide substantially new information from a view direction perpendicular to the initial one, but still are reasonably accessible for many eye-in-hand arrangements. Any pose from a depth less than the object’s depth will probably see common parts of the object as the frontal initial view.

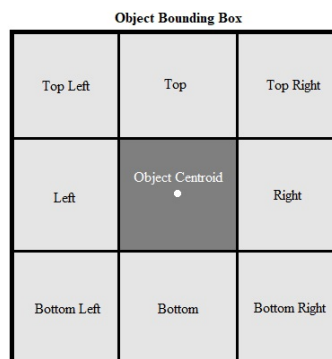


Figure 1: Tiling routine in the proposed next best view system.

In contrast, any pose with a depth farther than the object will see behind the object, which can be desirable, but has two disadvantages. First, it is hard to reach by a robotic system. Many robotic arms do not have the degrees of freedom required to move an arm-mounted camera to a pose facing the back of the object, as well as to poses at a large distance from the robot. It is also challenging to plan for a pose behind an object for a freely moving camera unit as the object’s thickness is unknown in a single frontal shot. The second reason is that for a single NBV based on the current frontal view of an object, we are not aware of the worthiness of the self-occluded area behind the object for active recognition camera poses. Therefore, the option of seeing behind an object is not considered as a candidate for a next viewpoint.

### 2.1 Local Analysis of the Current View

In the proposed method, the object bounding box, emerging from any object detection system, is divided into different regions. The tiled regions cover the entire area of the bounding box in a non-overlapping fashion. Figure 1 illustrates the tiling scheme in the proposed method. Each bounding box is divided into nine regions in the current implementation, where each of the eight peripheral tiles corresponds to one of the pose groups of a camera around the object. For instance, the top left tile represents a point of view when the camera is viewing the object from the object’s top left with the same depth to the camera as the object itself in the camera coordinate of the initial view. The camera in the new orientation can be placed arbitrarily close to the object considering the pose feasibility for the camera setup and the image resolution of the camera. Figure 2 shows this example situation.

The rationale behind this tiling scheme is that analyzing each region of the current view can reveal clues to a more informative NBV corresponding to the side of the object it is representing. In con-

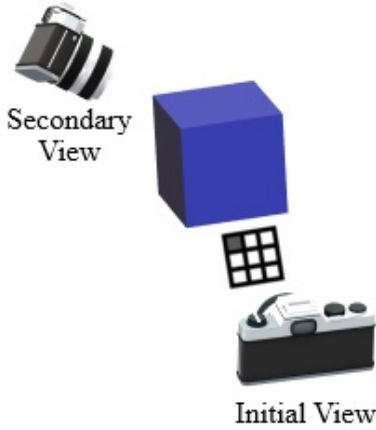


Figure 2: An example next viewpoint selection situation, where the top left tile is selected and consequently the secondary viewpoint is looking at the object from its top left.

trast to methods of (Potthast and Sukhatme, 2011), (Potthast and Sukhatme, 2014), (Doumanoglou et al., 2016), (Rebull Mestres, 2017), (Krainin et al., 2011), and (Bircher et al., 2016) that simply attempt to look at unobserved voxels, the proposed approach tries to further qualify its decision based on what is currently being seen. Additionally, the proposed method differs from techniques of (Wu et al., 2015) and (Doumanoglou et al., 2016) that hypothesize the object shape, as it only utilizes limited cues directly available in the initial view, instead of requiring the inference of explicit information about the entire shape, appearance, and relative pose of the object.

## 2.2 The Ensemble of Viewpoint Criteria

In the proposed method an equally weighted voting mechanism among four criteria selects the peripheral tile with the highest votes. Only a single vote is cast for the tile with the highest score from each criterion. Two of the criteria statistically analyze the texture of a tile. Another one evaluates the foreshortening of the object to estimate how visible its surface was in the initial view. The last criterion considers the classification dissimilarity between a tile and the entire object. In the following three subsections, we explain in detail the 4 voting criteria.

### 2.3 Statistical Texture Metrics

One of the instances where active vision proves to be helpful is when the object being observed is not clearly recognizable due to occlusion, lighting conditions, object shape, etc. One way to confront these situations can be to shift the view toward poses that are likely to be well-lit and provide better quality im-

ages. To this end, the second and third moment texture analysis tools are utilized. The two criteria are chosen to be obtained from the intensity histograms of each tile’s image to help in their faster processing.

#### 2.3.1 Second Moment (Variance) of Histogram

A high-contrast image has a higher chance of containing more features than a uniform one. The second moment or variance of intensity histogram is a measure of contrast of an image (Gonzalez, 2018). The variance of an intensity histogram is defined in (1) (Gonzalez, 2018).

$$\sigma^2(z) = \mu_2(z) = \sum_{i=0}^{L-1} (z_i - m)^2 p(z_i) \quad (1)$$

In the equation,  $\sigma^2(z)$  is the variance of intensity levels ( $z$ ), which is identical to the second moment,  $\mu_2(z)$ . In Addition,  $L$  represents the total number of intensity levels in the histogram,  $i$  is the index of the current intensity level,  $p(z_i)$  is the probability of an intensity level, and  $m$  is the mean of intensities, computed as follows:

$$m = \sum_{i=0}^{L-1} z_i p(z_i) \quad (2)$$

To scale the metric to the range of  $[0, 1)$ , the contrast score  $V(z)$  is calculated via (3).

$$V(z) = 1 - \frac{1}{1 + \sigma^2(z)} \quad (3)$$

The scaled second moment,  $V(z)$ , should be high ideally, because a greater  $V(z)$  means higher contrast and perhaps more features, with which a tile can be a cue to a feature-rich sideward surface for a good next viewpoint.

#### 2.3.2 Third Moment of Histogram

The third moment can be used as a way to measure how skewed is a histogram towards dark or bright levels (Gonzalez, 2018). It is defined in (4).

$$\mu_3(z) = \sum_{i=0}^{L-1} (z_i - m)^3 p(z_i) \quad (4)$$

A positive  $\mu_3(z)$  indicates a histogram with more probable bright intensity levels. A histogram weighing more towards darker intensities is also expected with a negative third moment. Therefore, to find a well-lit surface that is neither bright nor dark, we can seek for a third moment close to zero. Good lighting in a boundary tile may signal the existence of the

same condition for the corresponding side of the object, which is desirable. Equation (5) is introduced in the following to translate preferable lighting conditions to a higher score. In (5), higher  $L(z)$  values are related to close to zero third moments, while lower  $L(z)$  can be a result of large or small third moments.

$$L(z) = \frac{1}{1 + |\mu_3(z)|} \quad (5)$$

## 2.4 Foreshortening Score

Considering that we examine all criteria on the periphery tiles of an object's bounding box, an object surface with less foreshortening probably means that it should be easily visible to the sensor in a peripheral tile. However, in that case, since the peripheral surface has less perspective to the camera's image plane and its plane is on average closer to being parallel to the camera, there should be other faces of the object that are not being viewed by the camera. On the other hand, a peripheral surface with a perspective to the current view, is likely not clearly visible in the current view as its surface is tilted and exhibits foreshortening too. Based on this idea, the foreshortening score considers how much foreshortening is present, or in other words how parallel is the object surface being seen in a tile to the image plane of the 3D camera observing the object. Assuming the depth map of a tile is segmented, and the object surface constitutes the foreground pixels, the foreshortening score is defined in the following:

$$P = - \frac{\sum_{p \in F} N \left( \left( \frac{dz}{dx_p}, \frac{dz}{dy_p}, 1 \right) \cdot \vec{z} \right)}{|F|} \quad (6)$$

where  $P$  is the foreshortening score,  $p$  is a pixel in the current tile,  $F$  is the set of foreground pixels,  $|F|$  shows the number of pixels in the tile that are designated as foreground,  $N()$  stands for a function to normalize a vector, and  $\vec{z}$  is the depth axis in the initial view's camera coordinate. The derivatives of depth ( $z$ ) with respect to  $x$  and  $y$  axes in the initial view's pixel coordinate are calculated for a particular pixel  $(x_p, y_p)$  in the following way:

$$\frac{dz}{dx} \Big|_{x=x_p} = z(x_p + 1, y_p) - z(x_p - 1, y_p) \quad (7)$$

$$\frac{dz}{dy} \Big|_{y=y_p} = z(x_p, y_p + 1) - z(x_p, y_p - 1) \quad (8)$$

The  $z(\cdot, \cdot)$  in (7) and (8) signifies the depth at a pixel of the depth map. To obtain a depth map, the

initial viewpoint must be captured by a 3D camera. It is common for ordinary 3D cameras to produce small fragments of unknown values spread over their generated depth map. To resolve this issue, the maximum depth in the current tile is replaced over all the unknown values. We are assuming that large depth values are attributed to the background. To eliminate the background from affecting the score, only the foreground areas ( $F$ ) obtained through Otsu's segmentation (Otsu, 1979) are used in (6).

For every foreground pixel in the depth map the term  $N \left( \left( \frac{dz}{dx_p}, \frac{dz}{dy_p}, 1 \right) \right)$  in (6) computes the normalized surface normal. The inner product of the surface normal and the  $z$  axis of the camera coordinate measures how parallel are the object surface and the image plane of the camera in the initial view, effectively quantifying the foreshortening of the object. Ultimately, to find the average parallelism of the object surface to the camera, the results of the inner products are averaged over all the foreground pixels. The proposed score prefers a tile when its score is higher.

## 2.5 Tile Classification Dissimilarity

When an AOR system is uncertain about its recognition, it can be a good idea to find where in the initial view (i.e. which tile) is contributing more to the uncertainty by not confirming the initial view's recognition. Later, trying to take a new look from the direction of that opposing tile will probably help in getting new information and resolving the ambiguity. Accordingly, to measure the extent of dissimilarity of class probabilities of the whole object image and a tile, the sum of their absolute differences (SAD) is used. This criterion is defined in (9).

$$S_j = \sum_{i \in G} \left| p_{ij}^{c_j}(i) - p_o^c(i) \right| \quad (9)$$

where  $S_j$  is the dissimilarity score between the tile  $j$  and the complete object image,  $G$  represents the set of object classes, and  $p_{ij}^{c_j}(i)$  and  $p_o^c(i)$  are probabilities of a class  $i$  after classifying the tile  $j$  and the whole object image by the classifiers trained for tile  $j$  ( $c_j$ ) and the whole object ( $c$ ), respectively. The  $c$  and  $c_j$  are conventional classifiers, trained with color images of objects, with the difference that  $c_j$  only uses the portion of images related to tile  $j$ , while  $c$  considers the whole object images in the training.

## 3 EXPERIMENTAL RESULTS

The proposed next best view method was evaluated on a dataset we created, particularly for benchmarking of

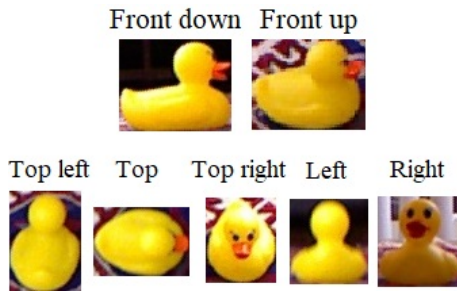


Figure 3: A sample situation in the dataset.

active object recognition techniques. To produce uncertain initial recognitions that cause an active object recognition system to trigger, the initial views of objects were intentionally distorted in the tests. In addition, the tests were performed on AOR systems with different classifiers and fusion methods to ensure the results are not biased for a specific type of AOR system.

### 3.1 The Test Dataset for Active Object Recognition

We collected 240 test situations, generally for evaluating active recognition systems, especially next best view methods. The dataset is comprised of 10 objects, each one being shown in 24 situations. The objects in each of their 24 test situations were placed in various poses (4 random faces of the object), lighting conditions (2 modes: darker and brighter), and background textures (3 modes: dark tabletop, light carpet, and colorful rug). There are seven images and their corresponding depth maps in each situation: one for a frontal initial view, another for an initial view with a slightly higher altitude initial view, and five others for the images/depth maps taken from the sides of objects as follows: left, top left, top, top right, and right. Figure 3 shows a sample situation for one of the objects in the dataset. The dataset is published along with the current paper.

### 3.2 Emulating AOR Triggering Conditions

Active object recognition systems are normally used when the classifiers suffer reduced performance due to occlusion or unfavorable perspective of objects. Because the initial views in the test dataset are clear and unobstructed, the initial views are altered to create the conditions that can trigger AOR. These alterations are superimposing a corner of the image and its respective depth map, amounting to 36% of their area, by a patch of another randomly selected object image

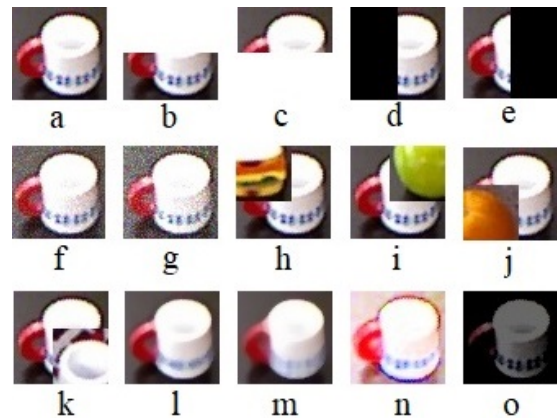


Figure 4: Initial view distortions. a) Original image, b, c) Top/bottom whiteout, d, e) Left/right blackout, f, g) Lighter/heavier noise, h, i, j, k) Corner superimpose, l, m) Lighter/heavier blur, n) Bright, o) Dark.

and its depth map, replacing with white or black an entire half of the image and its corresponding depth map, Gaussian blurring in two levels, adding noise in two levels, and image brightening/darkening.

The tests were performed on the original images and their altered versions as well as their corresponding depth maps, totaling 15 test scenarios for any test situation in the dataset. Figure 4 shows the 15 versions of the initial view for an object in a sample situation.

### 3.3 Test Benchmarks

Since there are two initial images in each test situation in the dataset, two experiments can be performed for a single situation. As mentioned in the former section, for each initial image 15 test scenarios with various alterations are possible. Therefore, 30 tests are performed for any test situation. With the existence of 240 test situations in the dataset, 7200 situations were evaluated for any vision system in the tests.

To ensure that the proposed NBV is independent of the classifier and the fusion algorithms in the AOR system, five different classifiers and three fusion techniques were examined in order to take their average results. Averaging, Naïve Bayes (Hoseini et al., 2019a), and Dempster-Shafer (DS) (Hoseini et al., 2019b) fusion algorithms are used in the tests. Three of the classifiers are Convolutional Neural Network (CNN) models with different number and composition of layers, activation functions, and pooling operations. Another one is a Support Vector Machine (SVM) classifier with the feature vector comprised of Hu moments of the three RGB (red-green-blue) planes, besides the reduced Histogram of Oriented Gradients (HOG) of the gray level image of the in-

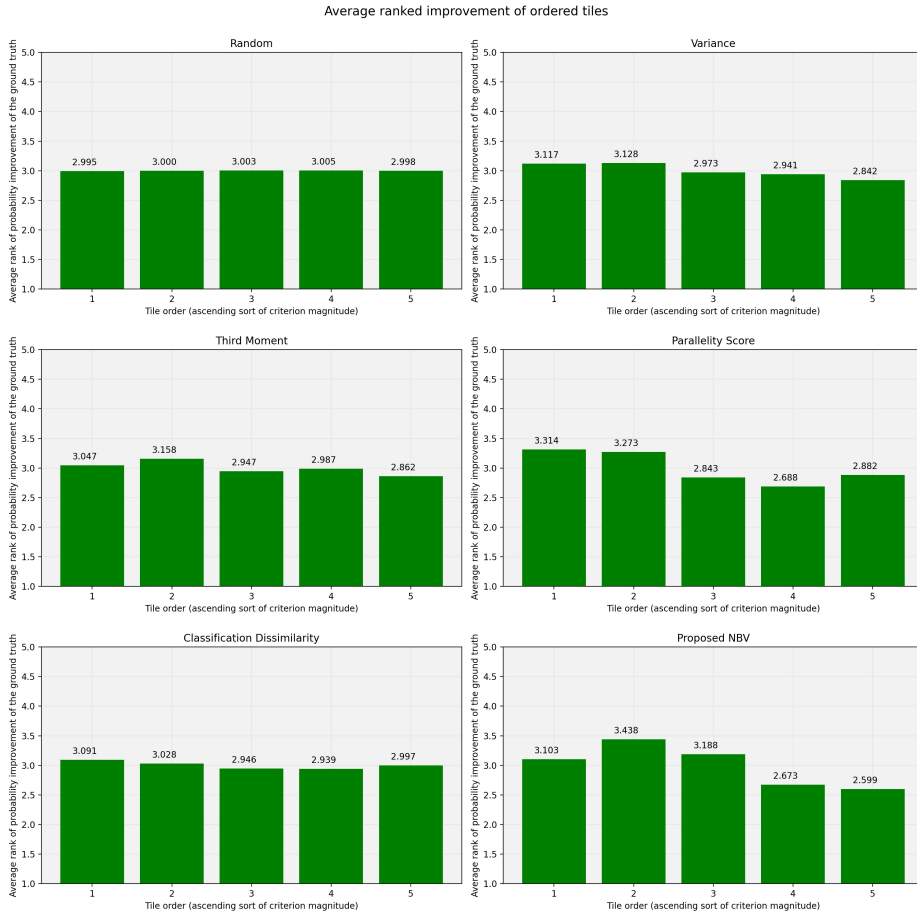


Figure 5: Average ranked improvement of tiles in ascending order of scores.

put. The last one is a random forest that uses a bag of visual words of Speeded Up Robust Features (SURF) keypoint descriptors.

Considering the possible combinations of the classification and fusion approaches, 15 benchmarks were evaluated, each with 7200 situations tested. In the tests, the confidence threshold of the AOR, explained in (Hoseini et al., 2019a) and (Hoseini et al., 2019b), was set to 20, that means the second viewpoint is retrieved if the highest class probability of the initial view is less than 20 times of the second highest one.

### 3.4 Obtained Results

#### 3.4.1 Ranked Ground Truth Improvement

In every test situation, the five prospective next viewpoints are examined for the scores they get from every criterion. In Figure 5, the tiles are sorted on the horizontal axis in an ascending order of the scores of each designated criterion. The height of the bars for any tile shows the mean rank of the tile in attaining better

probability for the ground truth classes after the decision fusion stage. The lower the rank and the closer it is to 1, the better it is. Therefore, in Figure 5 it is desirable to have lower height of the bars in the right sides of the plots.

From the results, it can be seen that the proposed NBV method attains better ranks for the tiles it scores higher. It means that it is useful in selecting the viewpoints that offer the best improvement in probability of the true class in the AOR system's output. Additionally, Figure 5 shows the performance of randomly selecting the next view and the individual criteria that are part of the ensemble. All the proposed individual criteria in the ensemble mostly find the better tiles with their scorings and tend to bring the height of their very right bar down, despite being not as good as the combination of them, which causes sharper decline in the height of the right bar.

#### 3.4.2 Performance per Criterion

Figure 6 compares the ratio of accuracy, precision, recall, and  $F_1$  score improvement of the proposed sys-

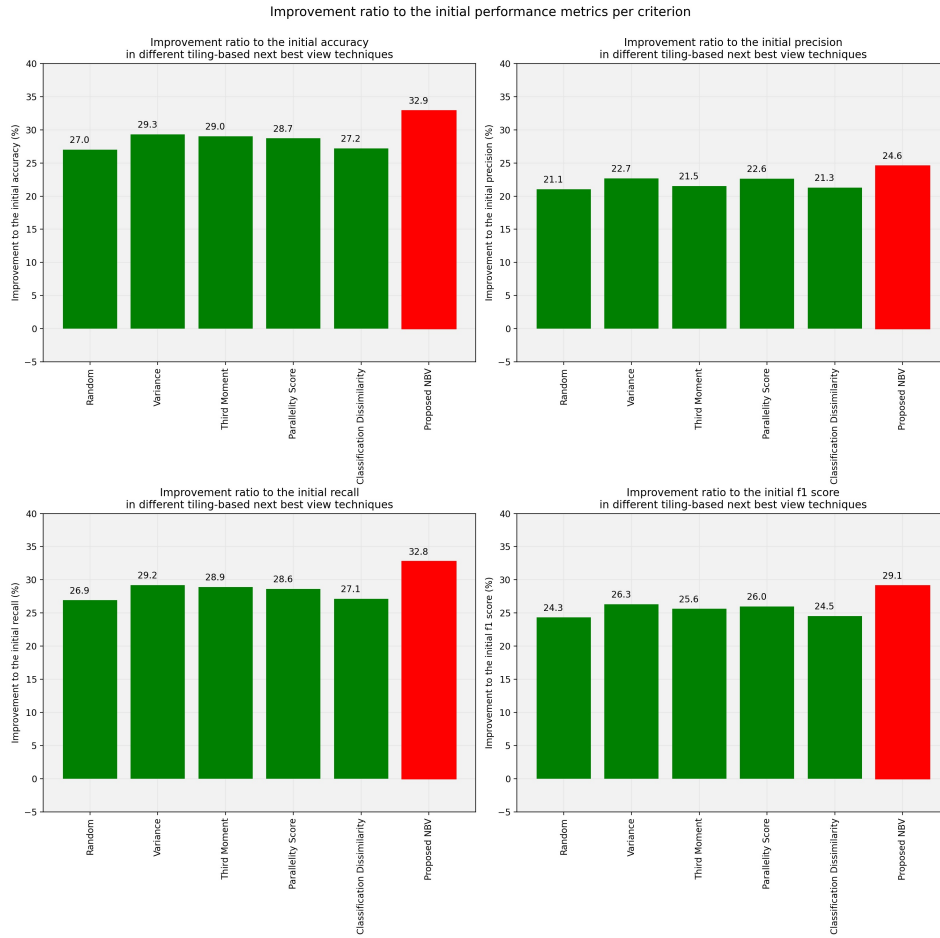


Figure 6: Improvement ratio to the initial performance metrics per measure.

tem and its constituting measures as well as random view selection to their initial performance metrics. We see that the proposed system achieves high improvements and is better than the other criteria in the figure, including the random selection of next viewpoint. Accuracy and  $F_1$  score of the proposed method is 5.9% and 4.8% more than a randomly viewpoint selecting AOR system.

### 3.4.3 Performance Improvement per Sorted Tiles

The accuracy, precision, recall, and  $F_1$  score improvement of the AOR system by using any of the five possible tiles in the tests are shown in Figure 7. The tiles are sorted in the horizontal axis based on the scores they receive from each measure. It is desirable to see better performance for the tiles the NBV system emphasizes more, i.e. the ones with higher scores in the right side of each plot. Therefore, we want to see higher bars on the right side of each plot. The results prove that the proposed NBV is effective in ob-

taining higher performance indices in its top picks. The individual measures participating in the ensemble also show a trend of increasing accuracy, precision, recall, and  $F_1$  score with the higher scores they produce, which is not always true for the random selection.

### 3.4.4 Receiver Operating Characteristic (ROC) Curves

Figure 8 shows the ROC curves obtained through micro-averaging for all the samples in the 15 benchmarks. The blue curves in the figure, show the results of the initial view recognitions only, while the green curves indicate the effect of fusing with the results of a randomly selected view. The red curves, instead, show the results of utilizing the proposed method. Comparing the three sets of the curves verifies the effectiveness of the AOR system in enhancing the ROC curve, and of the NBV method in increasing the recognition improvement.

Performance metrics improvement of ordered tiles

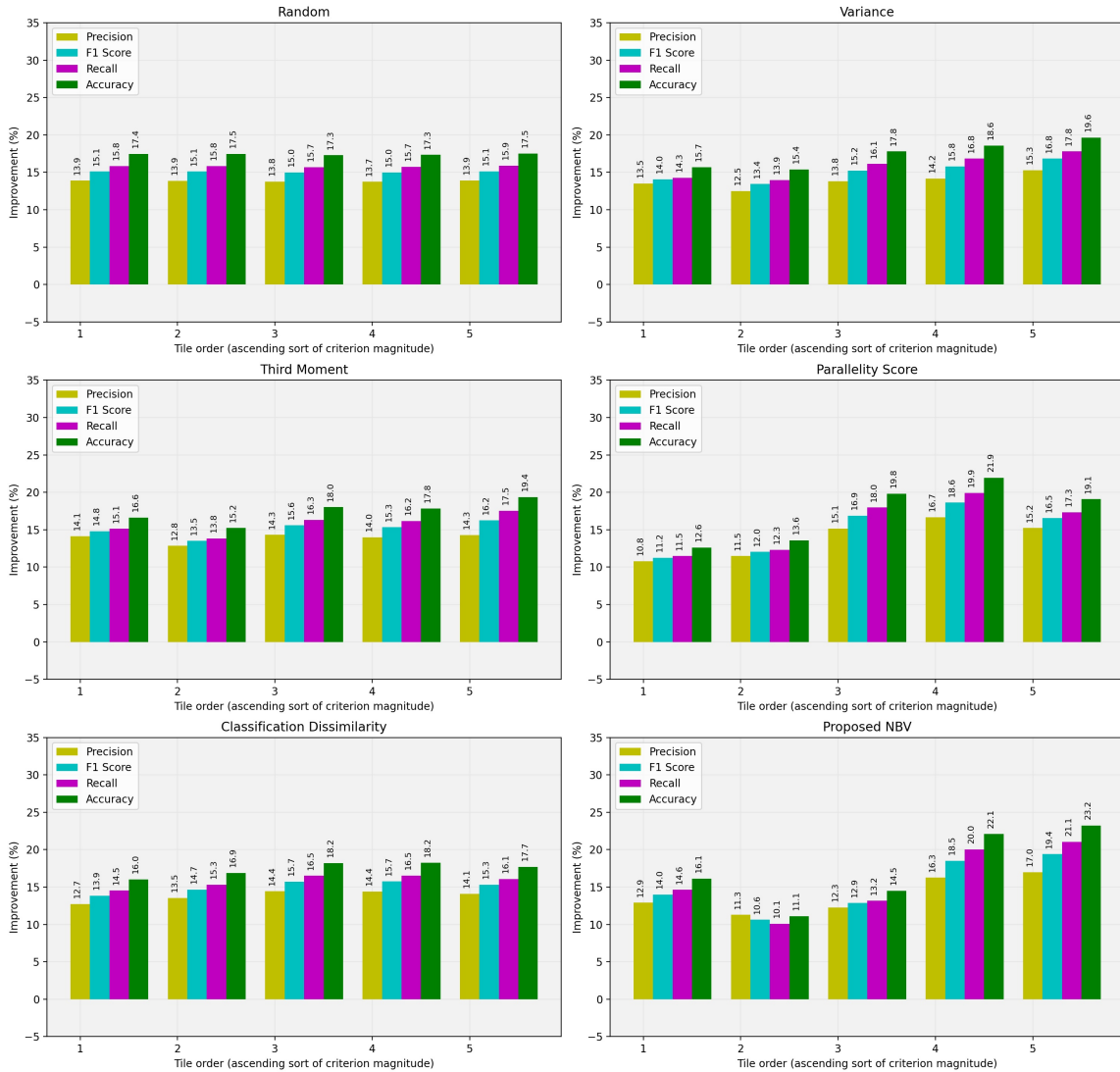


Figure 7: Performance metrics improvement of tiles in ascending order of scores.

### 3.5 Discussion

The experimental results clearly show the applicability of the proposed NBV in improving accuracy, recall, precision, and thus  $F_1$  score of the active object recognition systems. In the results, we observe that the active object recognition systems with a random selection of next viewpoint attain 27% and 24.3% accuracy and  $F_1$  score improvement on average. With the proposed next best view method, the same AOR systems experience 32.9% and 29.1% accuracy and  $F_1$  score enhancements, which amounts for 5.9% and 4.8% further improvement over a random AOR. Interestingly, the tile ranking using the foreshortening score shows that sometimes the tiles with the penul-

imate score reach better ranks than the highest scoring ones. Those cases occur perhaps when the higher scoring tile has a very steep object surface with respect to the image plane of the camera in the initial view. Compared to less steep surfaces, a very steep one may impede the proper view of the respective object side from the perspective of the initial view.

## 4 CONCLUSION

In this paper a next best view approach for active object recognition systems was presented. The proposed view selection divides an initial image of an object

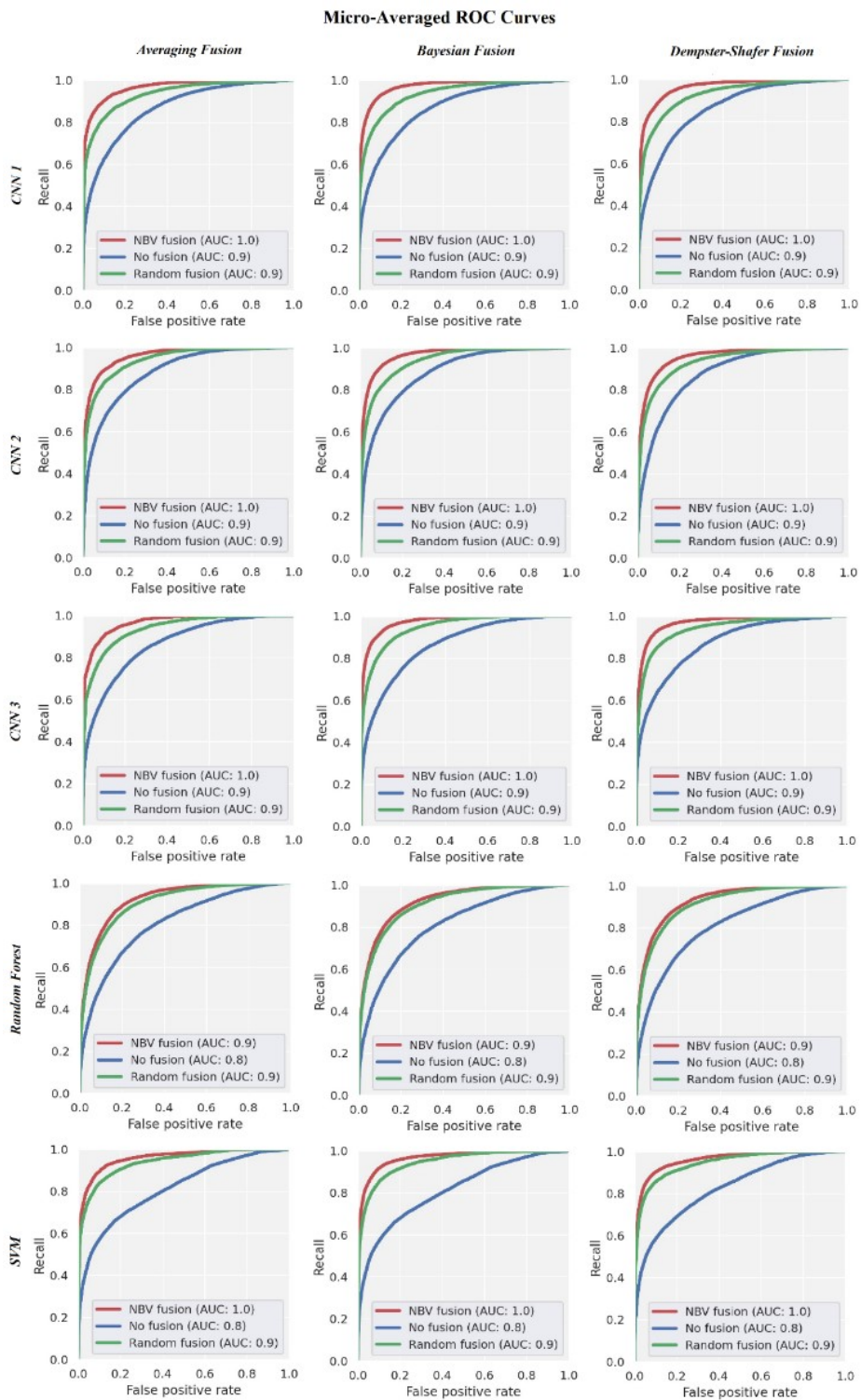


Figure 8: ROC curves of different test benchmarks.

into a few zones to investigate each one for clues in determining better next views. Each area is analyzed through an ensemble of four different techniques:

foreshortening, histogram variance, histogram third moment, and classification dissimilarity. There is no need to a prior training set of specific views of ob-

jects or their 3D models in the proposed method. It can suggest the next viewpoint based on just the information of a single initial view, which along with the property of considering both the 3D shape and appearance of objects offers an intrinsic advantage for active object recognition tasks.

A dataset for testing active object recognition systems was developed as a part of this work and was used to evaluate the proposed next best view technique. In the presence of heavy occlusions in the initial view, we report 32.9% and 29.1% average accuracy and  $F_1$  score improvements compared to the initial performance values.

In continuation to this work, future efforts should be directed toward probing alternative tiling schemes of the initial view. Another area of work can be investigating other ensemble methods in place of the current voting scheme. A meta-learning approach would be a potentially interesting way to combine the tile scores.

## ACKNOWLEDGMENTS

This work has been supported in part by the Office of Naval Research award N00014-16-1-2312 and US Army Research Laboratory (ARO) award W911NF-20-2-0084.

## REFERENCES

- Atanasov, N., Sankaran, B., Le Ny, J., Pappas, G. J., and Daniilidis, K. (2014). Nonmyopic view planning for active object classification and pose estimation. *IEEE Transactions on Robotics*, 30(5):1078–1090.
- Barzilay, O., Zelnik-Manor, L., Gutfreund, Y., Wagner, H., and Wolf, A. (2017). From biokinematics to a robotic active vision system. *Bioinspiration & Biomimetics*, 12(5):056004.
- Bircher, A., Kamel, M., Alexis, K., Oleynikova, H., and Siegwart, R. (2016). Receding horizon” next-best-view” planner for 3d exploration. In *2016 IEEE international conference on robotics and automation (ICRA)*, pages 1462–1468. IEEE.
- Doumanoglou, A., Kouskouridas, R., Malassiotis, S., and Kim, T.-K. (2016). Recovering 6d object pose and predicting next-best-view in the crowd. In *Proceedings of the IEEE conference on computer vision and pattern recognition*, pages 3583–3592.
- Gonzalez, R. C. (2018). *Richard E. Woods Digital Image Processing*, Pearson. Prentice Hall.
- Hoseini, P., Blankenburg, J., Nicolescu, M., Nicolescu, M., and Feil-Seifer, D. (2019a). Active eye-in-hand data management to improve the robotic object detection performance. *Computers*, 8(4):71.
- Hoseini, P., Blankenburg, J., Nicolescu, M., Nicolescu, M., and Feil-Seifer, D. (2019b). An active robotic vision system with a pair of moving and stationary cameras. In *International Symposium on Visual Computing*, pages 184–195. Springer.
- Jia, Z., Chang, Y.-J., and Chen, T. (2010). A general boosting-based framework for active object recognition. In *British Machine Vision Conference (BMVC)*, pages 1–11. Citeseer.
- Krainin, M., Curless, B., and Fox, D. (2011). Autonomous generation of complete 3d object models using next best view manipulation planning. In *2011 IEEE International Conference on Robotics and Automation*, pages 5031–5037. IEEE.
- Otsu, N. (1979). A threshold selection method from gray-level histograms. *IEEE transactions on systems, man, and cybernetics*, 9(1):62–66.
- Paul, S. K., Chowdhury, M. T., Nicolescu, M., Nicolescu, M., and Feil-Seifer, D. (2020). Object detection and pose estimation from rgb and depth data for real-time, adaptive robotic grasping. In *24th International Conference on Image Processing, Computer Vision, & Pattern Recognition (IPCV)*. Springer.
- Pothast, C. and Sukhatme, G. S. (2011). Next best view estimation with eye in hand camera. In *IEEE/RSJ Intl. Conf. on Intelligent Robots and Systems (IROS)*. Citeseer.
- Pothast, C. and Sukhatme, G. S. (2014). A probabilistic framework for next best view estimation in a cluttered environment. *Journal of Visual Communication and Image Representation*, 25(1):148–164.
- Rebull Mestres, J. (2017). Implementation of an automated eye-in hand scanning system using best-path planning. Master’s thesis, Universitat Politècnica de Catalunya.
- Wu, Z., Song, S., Khosla, A., Yu, F., Zhang, L., Tang, X., and Xiao, J. (2015). 3d shapenets: A deep representation for volumetric shapes. In *Proceedings of the IEEE conference on computer vision and pattern recognition*, pages 1912–1920.